# Super-resolution optical microscopy based on photonic crystal materials

Igor I. Smolyaninov and Christopher C. Davis
*Department of Electrical and Computer Engineering, University of Maryland, College Park, Maryland 20742, USA*

Jill Elliott, Gregory A. Wurtz, and Anatoly V. Zayats
*School of Mathematics and Physics, The Queen's University of Belfast, Belfast BT7 1NN, United Kingdom*
(Received 20 May 2005; published 18 August 2005; publisher error corrected 19 August 2005)

Theoretical model of the enhanced optical resolution and the principles of subdiffraction imaging using two-dimensional photonic and plasmon-polaritonic crystals is presented based on the properties of electromagnetic Bloch waves in periodic structures. The super-resolution is achieved due to coupling of evanescent components of the diffraction field generated by the object to the propagating Bloch modes of the photonic crystal space. The resolution enhancement is shown to occur in a general case of photonic-crystal-type materials with either positive or negative effective refractive index. Both signs of the effective refractive index have been observed in the imaging experiments with surface polaritonic crystals, in which individual virus imaging has been achieved.

DOI: 10.1103/PhysRevB.72.085442 PACS number(s): 78.67.−n, 78.20.Ci, 42.70.Qs

## I. INTRODUCTION

High-resolution optical imaging attracts constant attention due to its important applications in material science, biology, photolithography, etc. Development of far-field optical techniques capable of subdiffraction resolution has recently progressed fast due to concepts applied to image formation such as negative refraction materials,[1] surface plasmon polariton assisted imaging,[2] and in the case of fluorescent objects, saturated depletion of stimulated emission.[3]

One of the approaches applicable to achieving optical super-resolution is based on the idea of a "perfect lens" made from an artificial negative refractive index metamaterial (or a thin silver film).[1,4] The "perfect lens" schemes have not yet achieved optical magnification in the experiment [however, a theoretical scheme which exhibits magnification in the electrostatic (near-field) regime has been described[5]]. Until metamaterials with negative permeability in the optical spectral range will be developed, an image formed by a "perfect lens" of thin metallic film can be observable only in the near field with scanning probe microscopy.

The successful scheme of far-field optical microscopy beyond the diffraction limit[2,6] is based on the two-dimensional (2D) surface polaritonic crystals[7] and utilizes surface plasmon polaritons (SPPs) generated over the periodic nanohole array made in thin metal film. In this arrangement, a parabolic dielectric droplet deposited onto a metal surface behaves as a magnifying mirror for large-wave-vector (short-wavelength) SPPs, which enables imaging not limited by diffraction of illuminating light.

Both the SPP based and the "perfect lens" microscopy provide optical resolution of the order of 60 nm. Since the conceptual designs of both the SPP assisted and the "perfect lens" microscopy schemes do not look much more complicated than the design of a regular far-field optical microscope (see Refs. 2 and 6, where the SPP-assisted microscope design is described in detail), they promise great potential in optical nanolithography and medical and biological imaging. Good understanding of the basic physics of these microscopy techniques is absolutely essential for making these microscopes into reliable and useful laboratory tools.

In this paper, we discuss the principles of subdiffraction imaging using 2D and three-dimensional (3D) photonic and plasmon-polaritonic crystals. First, we consider imaging properties of photonic and polaritonic crystals that are used in image formation. The subwavelength optical resolution can be achieved due to coupling of evanescent components of the diffraction field generated by the object to the propagating Bloch modes of the photonic crystal. Next, we present experimental images of various subwavelength test patterns, which are obtained using 2D plasmon-polaritonic crystals in both positive and negative refractive index regimes. In these experiments imaging has been achieved using curved SPP mirrors and properties of SPP Bloch waves traversing SPP crystal boundary. Finally, optical visualization of a T4 phage virus is demonstrated as an example of application of this technique to biological samples.

## II. IMAGING THROUGH PHOTONIC CRYSTAL SPACE

Before we describe any real experimental geometry of far-field optical microscopy based on 2D photonic crystal material, let us consider the transmission of electromagnetic waves with various spatial frequencies generated at a luminous object by an infinite "photonic crystal space." In the following simple numerical example, we use a test object which consists of two luminous dots separated by a gap [Fig. 1(a)]. The Fourier spectrum of this object is shown in Fig. 1(b). If the angular spectrum of spatial frequencies available for probing in the far field of the object with an optical apparatus (e.g., microscope objective lens) is limited by some maximum wave vector $k_{max}$ [represented by a circle of radius $k_{max}$ shown in Fig. 1(b)], the free (empty) space between the object and the lens behaves as a spatial frequency filter, which removes the spatial frequencies corresponding to evanescent waves. Thus, whatever optical design is implemented to collect the electromagnetic waves propagating

 

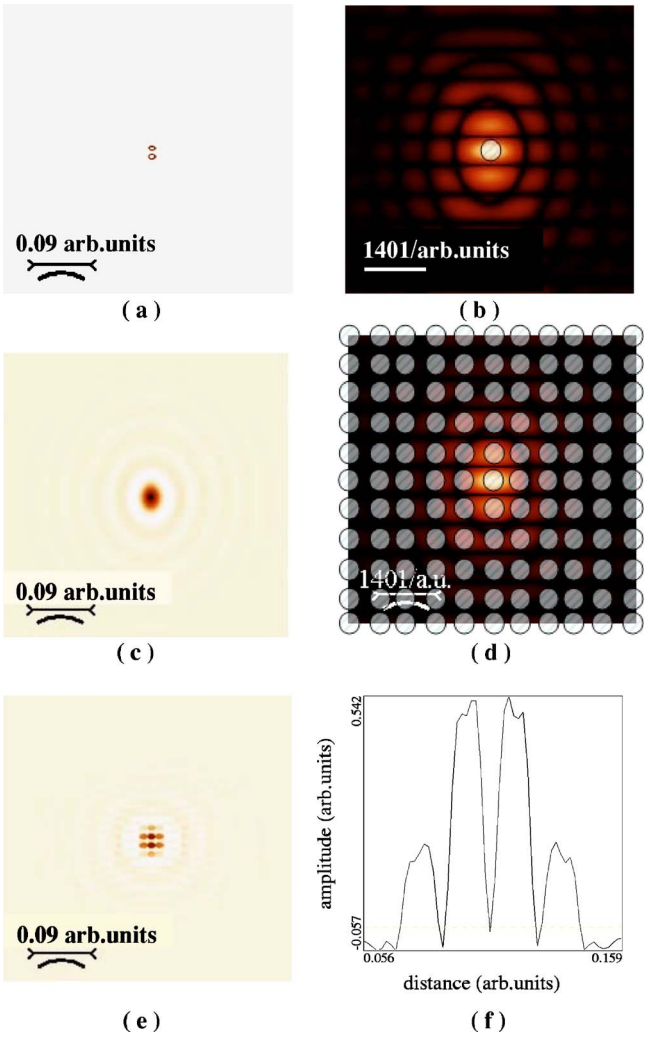


FIG. 1. (Color online) (a) A test object which consists of two luminous dots separated by a gap. (b) The Fourier transform of the object shown in (a). An area of the spatial frequency spectrum of electromagnetic waves available to probe is shown by a circle. (c) The inverse Fourier transform of the portion of the spectrum inside the circle in (b). (d) The pass band of the "photonic crystal space" with square photonic crystal lattice. (e) The inverse Fourier transform of the spatial frequency spectrum inside the photonic crystal pass band. (f) Cross section of the image in (e) indicates recovery of the two-dot structure of the object.

from the object, the best image in the far-field region would result from the inverse Fourier transformation of the portion of the spectrum falling inside the circle in Fig. 1(b). As a result, a smeared image in Fig. 1(c) would be obtained. The two-dot structure of the original object is lost in this image.

If the same object is placed inside a "photonic crystal space," while the same part of the spatial frequency spectrum (limited by the $k_{\max}$ value) is available for far-field probing outside the photonic crystal, the points in the Fourier space separated by integer multiples of the inverse lattice vectors become equivalent to each other because of the photonic crystal periodicity. If we assume that the photonic crystal has a square lattice [Fig. 1(d)] and acts as a spatial filter, an image shown in Fig. 1(e) can be recovered, which is obtained by the inverse Fourier transformation of the portion of the original spectrum inside all the circles in Fig. 1(d). The original information about the two-dot structure of the object is recovered in this case [Fig. 1(e)] as seen from the cross section [Fig. 1(f)].

This simple numerical example demonstrates that a far-field optical microscope with resolution beyond the $\lambda/2$ diffraction limit of conventional far-field optics can be built using photonic crystal materials. However, in order to achieve subdiffraction-limited resolution an object should be placed inside or very near the photonic crystal. Such a microscope can be dubbed "an immersion microscope based on photonic crystal material."

The imaging properties of a periodic structure, such as a photonic crystal slab or surface polaritonic crystal can be described by considering properties of electromagnetic Bloch waves in a periodic structure,

$$\psi_{\vec{k}} = \sum_{\vec{K}} C_{\vec{k}-\vec{K}} e^{i(\vec{k}-\vec{K})\vec{r}}, \tag{1}$$

where $\vec{k}$ is the wave vector defined within the first Brillouin zone, and $\vec{K}$ represents all the inverse lattice vectors. The Bloch wave is capable of carrying spatial frequencies of an object, which would be evanescent in free space. It does not matter if the dispersion of some particular Bloch wave is negative or positive. What is important for microscopy, is that the Bloch waves should have sufficiently large $C_{\vec{k}-\vec{K}}$ coefficients at large $\vec{K}$. The Fourier spectrum $F_{\vec{\kappa}}$ of the test object $f(\vec{r})$ described in the example above, can be written in the usual way as

$$f_{\vec{r}} = \sum_{\vec{\kappa}} F_{\vec{\kappa}} e^{-i\vec{\kappa}\vec{r}}, \tag{2}$$

where $\vec{\kappa}$ is the wave vector in free space. The same spectrum of the object in terms of the Bloch waves [Eq. (1)] is given by

$$F_{\vec{k}} = \sum_{\vec{K}} F_{-\vec{k}+\vec{K}} C_{\vec{k}-\vec{K}}. \tag{3}$$

Thus, high spatial frequencies of the object shape $F_{-\vec{k}+\vec{K}}$ are carried into the far-field zone of the object by $C_{\vec{k}-\vec{K}}$ components with large $\vec{K}$. The limit $C_{\vec{k}-\vec{K}} \approx \text{const}$ is the most beneficial for super-resolution imaging. It corresponds to the photonic Bloch waves obtained in the tightly bound approximation, in which the photonic bands are very narrow. In this approximation, the amplitude of Bloch modes is most significant in the lattice nodes and simple considerations similar to spatial filtering through the holes placed in the lattice nodes can be applied as discussed above (Fig. 1).

In the case of imaging with surface plasmon polaritonic crystals based on SPP optics[2,6] this Bloch wave description agrees well with the model of short-wavelength SPPs[2,8] which are excited by the periodic nanohole array. Near the surface plasmon resonance the SPP dispersion is almost flat.

In order to be useful in far-field microscopy, a given photonic crystal geometry must exhibit image magnification to the extent that the image size should surpass the $\lambda/2$ diffraction limit of the usual far-field optics. Such a magnified im-

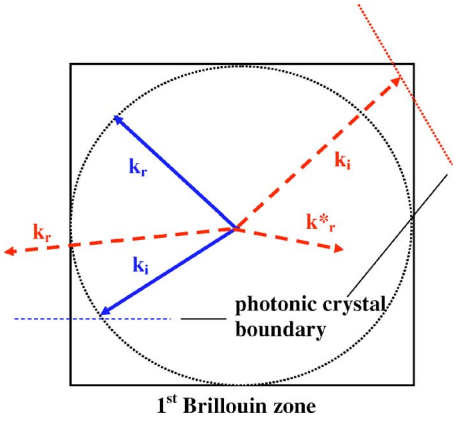


FIG. 2. (Color online) A Bloch wave reflection from a photonic crystal boundary. For incident wave vectors $\vec{k}_i$ inside the dashed circle the wave vector of the reflected Bloch wave $\vec{k}_r$ obeys the law of reflection. In the case of incident wave vectors located in the corners of the first Brillouin zone (outside the dashed circle) the $\vec{k}_r$ vector obtained according to the law of reflection must be shifted inside the first Brillouin zone by an addition of an inverse lattice vector. However, the obtained $\vec{k}_r^*$ and $\vec{k}_r$ directions of the Bloch wave propagation are physically equivalent in a periodic lattice.

age can be transferred to a free space region and viewed by a regular microscope. This means that some curved photonic crystal boundary should be used. Since refraction of photonic crystals depends very strongly on frequency, propagation direction, and other parameters (a superprism effect is well-known in photonic crystal geometries, see, for example, Refs. 9 and 10), a reliable photonic crystal lens geometry would be very difficult to predict theoretically and realize in the experiment. On the other hand, a reflective optics geometry seems to be a good practical solution. The law of reflection is observed for almost all wave vectors $\vec{k}$ within the first Brillouin zone for Bloch wave reflection from a planar photonic crystal boundary (Fig. 2). The Umklapp processes which occur in the corners of the Brillouin zone do not spoil the geometrical optics reflection picture because in a periodic lattice the $\vec{k}_r$ and $\vec{k}_r^*$ directions are physically equivalent, and they correspond to the same Bloch wave. If the reflecting boundary is slightly curved (so that the curvature radius is much larger than the period of the photonic crystal lattice) geometrical optics picture of reflection remains valid. Thus, a magnifying mirror can be designed using photonic crystal materials. This has been demonstrated in the experiments with surface plasmon polaritons described in Refs. 2 and 6 where the role of the mirror is played by the boundary of the dielectric droplet, which is placed on the surface of the periodic nanohole array in a gold film.

Once the image is magnified, it should be projected into free space (3D or 2D) outside the photonic crystal optical element (photonic crystal mirror, photonic crystal slab, etc.) so that it can be viewed. At this stage the refractive properties of the photonic crystal play an important role in image formation. As we shall see in the following sections of this paper, the sign of the effective refractive index of the photonic crystal defines the character of image magnification of the 2D optical system based on photonic crystal mirror.

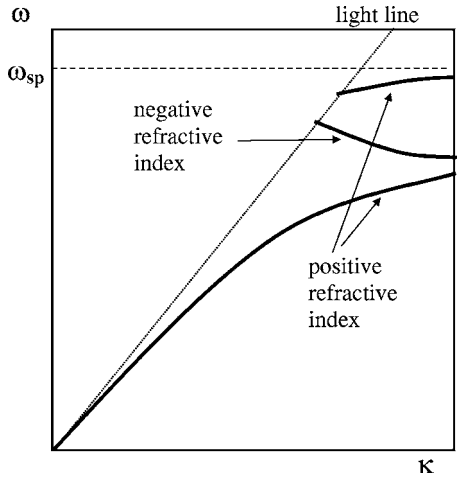


FIG. 3. Schematic view of the SPP dispersion in the first Brillouin zone.

## III. THE ROLE OF EFFECTIVE REFRACTIVE INDEX OF PHOTONIC CRYSTAL MIRROR IN IMAGE MAGNIFICATION

Since both 2D photonic crystal materials and surface polaritonic crystals exhibit similar electromagnetic band structures, we will consider SPP crystal to illustrate the behavior of the magnifying mirror (since it is directly related to the experiments discussed below). A typical dispersion of the SPP modes on a periodically modulated surface of a metal film in the vicinity of the surface plasmon resonance is shown schematically in Fig. 3. The examples of surface polariton dispersion on various 2D SPP crystals may be found in Refs. 11 and 12. It appears that the sign of the SPP group velocity may be either positive or negative depending on the Brillouin zone structure and SPP Bloch wave frequency (in fact, the SPP dispersion can be almost flat, especially in higher Brillouin zones which lie near the surface plasmon resonance frequency). As was shown above, the latter circumstance $C_{\vec{k}-\vec{K}} \approx \text{const}$ is advantageous for high-resolution imaging applications. On the other hand, the sign of the SPP group velocity defines the effective refractive index of the photonic crystal material in this frequency range.[13] According to calculations in Ref. 11, the sign of the SPP group velocity for a particular SPP Bloch mode branch is rather insensitive to the propagation angle, which means that the model of geometrical optics refraction (the Snell's law) is applicable to SPP propagation across the interface between the nanohole array region and a smooth metal film.

Let us consider the effect of this refraction on the image formation in the SPP-assisted microscope described in Refs. 2 and 6. As may be seen from Fig. 4, positive effective refractive index of the nanohole array causes some shift in the location of the image, which is formed by the SPP crystal mirror. On the other hand, negative refractive index would produce a much more drastic effect on the imaging properties of the mirror. A real image produced by the mirror, which would be located outside the nanohole array, becomes a virtual image due to negative refraction at the photonic crystal boundary (Fig. 4). However, if a real image produced

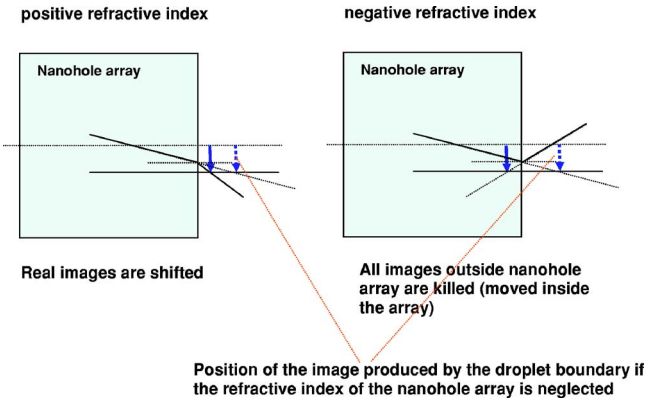


FIG. 4. (Color online) Effect of the sign of the effective refractive index of the SPP crystal on the image formation. Positive refractive index causes small shift in image location, while negative refractive index converts real images outside the SPP crystal into virtual ones.

by the mirror is located inside the nanohole array, negative refraction at the interface produces a second real image over the unperturbed metal film [Fig. 5(a)]. The character of refraction at the nanohole array boundary is clearly identifiable in the experiment. While positive refraction produces image magnification which grows with distance from the mirror along the optical axis of the system (this behavior has been

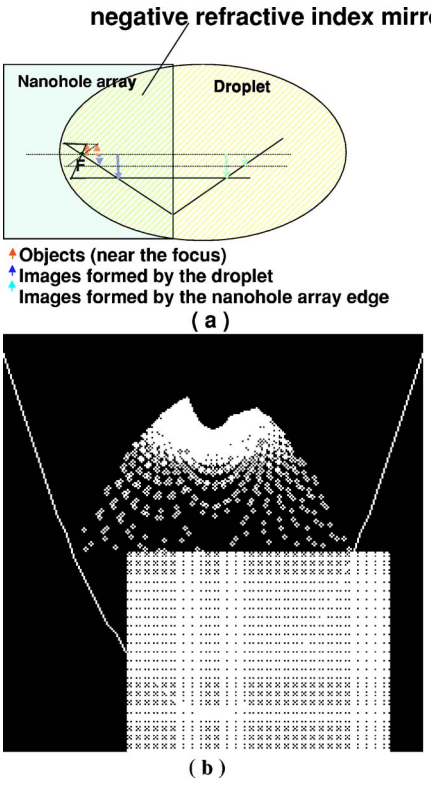


FIG. 5. (Color online) (a) The dependence of the magnification in images produced by the SPP crystal mirror with negative refractive index on the distance from the mirror edge. (b) Theoretical image of a triplet array of nanoholes (rectangular area at the bottom of the image) in the case of negative effective refractive index of the SPP crystal.

observed in our earlier experiments[2,14]), negative refraction produces an opposite behavior of magnification, image magnification is the highest in the immediate vicinity of the nanohole array boundary, and becomes smaller at larger distances along the optical axis. This may be seen from Fig. 5(b), which has been calculated in the case of a triplet nanohole array, which has a negative effective refractive index [compare this figure with Figs. 4(b) and 4(f) from Ref. 2, where experimental and theoretical images of a triplet nanohole array with positive refractive index were presented]. "Negative" behavior of the image magnification for some nanohole arrays has been indeed observed in our experiments, as described below.

## IV. EXPERIMENTAL OBSERVATIONS

The design and operation of our SPP-assisted immersion microscope is described in detail in Refs. 2, 6, and 14. We have used a two-stage microscope design in which a magnified planar image produced originally by surface plasmon polaritons in the metal surface plane is observed with a conventional optical microscope due to SPP coupling to light via random surface roughness or tailored surface of the periodic nanohole array. Glycerin microdroplets have been used as 2D magnifying mirrors for SPPs. Experiments were conducted using light of various wavelengths of an Ar-ion laser in the vicinity of 500 nm wavelength in air, which are located very close to the frequency of the surface plasmon resonance for a gold-glycerin interface. Since the SPP wavelength and the nanohole array period are much smaller than the droplet sizes, the image formation in such a magnifying mirror can be analyzed by simple geometrical optics. To check the imaging properties of the microscope, various arrangements of periodic nanohole arrays in metal films were studied. Illuminated by light at appropriate wavelength nanohole arrays excite the SPP modes on a structured surface of metal film.[7]

Resolution test of the microscope has been performed using $30\times30$ $\mu m^2$ arrays of singlet, doublet, and triplet nanoholes (Fig. 6) made in a gold film using focused ion beam milling (FIB) technique. In this experimental geometry the arrays exhibited positive refraction. All the test patterns shown in Fig. 6 had 100 nm hole diameter with 40 nm distance between the hole edges in the doublet and triplet structures, and 500 nm lattice period. All the structures were resolved in the optical images obtained using SPP-assisted microscopy. Cross-sectional analysis of these images performed in Refs. 2 and 14 indicates spatial resolution of the order of 60 nm. However, when the illuminating light wavelength is such that no SPP Bloch modes can be excited on the periodic arrays, the resolution is lost as should be expected.[2]

In the next series of experiments SPP-assisted imaging of aperiodic test samples has been studied. The aperiodic sample in Fig. 7(a) was made to emulate various nanometer-scale shapes, which may occur in real-life biological applications. Similar to earlier experiments, the boundary of the SPP mirror was positioned over the array of nanoscale holes

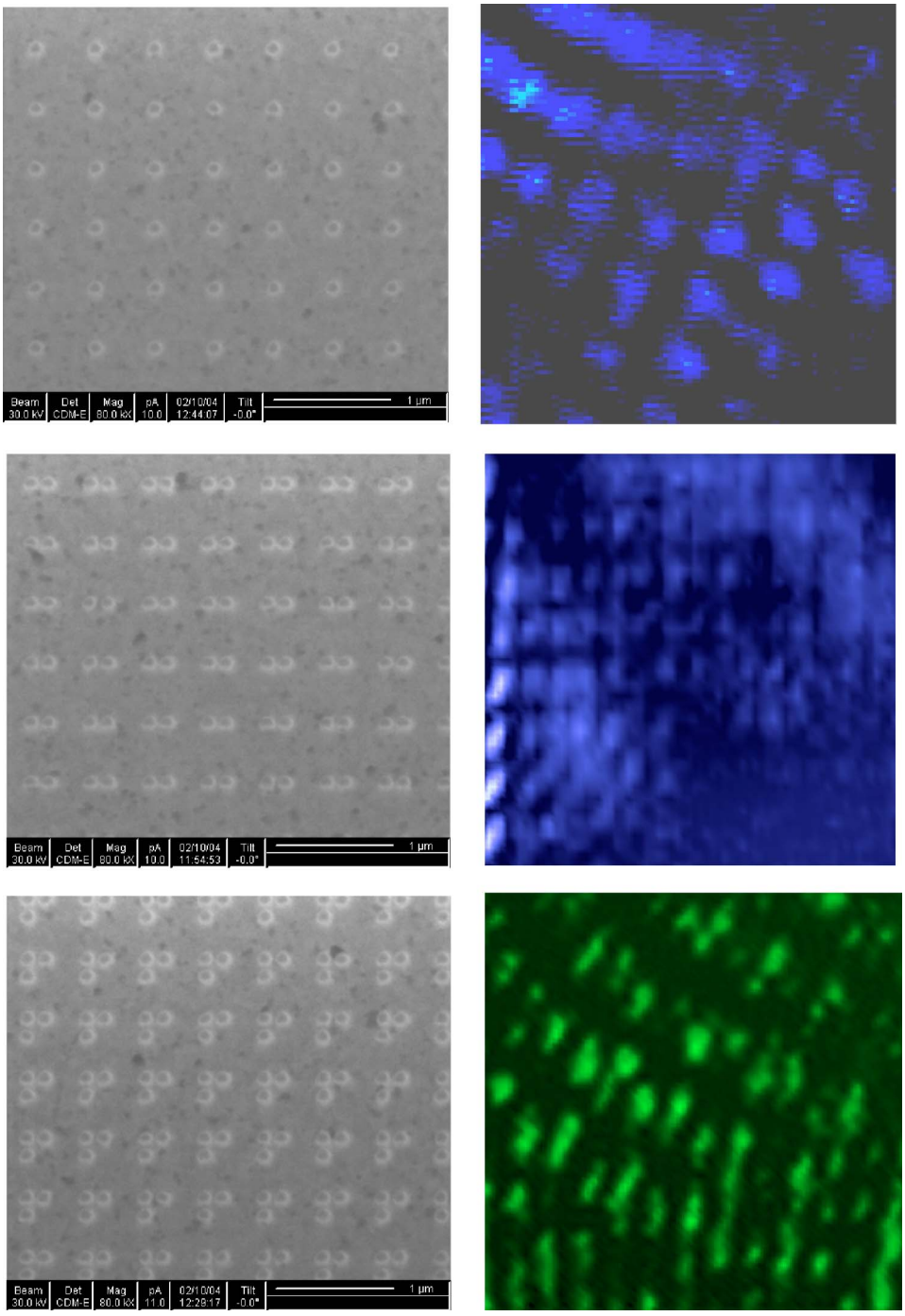


FIG. 6. (Color online) Resolution test of the microscope. The $30\times30\ \mu m^2$ arrays of singlet, doublet, and triplet nanoholes (100 nm hole diameter, 40 nm distance between the hole edges in the doublet and triplet, 500 nm period) shown in the left column are imaged using a SPP mirror formed by a glycerine droplet. The optical images on the right-hand column are obtained at $\lambda_0=502$ nm (singlets and doublets) and at $\lambda_0=515$ nm (triplets).

used as objects in the experiment. Illuminated with light, these nanoholes generate SPPs, which upon reflection from the droplet edge form magnified images of individual nanoholes over the unmodified area of the gold film [Fig. 7(b)]. Zoom of the image area, which is adjacent to the square array of nanoholes [Fig. 7(c)] indicates that individual elements of the aperiodic array have been imaged with various degree of success [image quality appears to be the best on the right-hand side of Fig. 7(c) where the shapes of individual nanoholes are clearly recognizable]. The images of the elements of the array are somewhat distorted due to their position with respect to the mirror (the same as in a conventional parabolic or elliptical mirror) and the degree of distortion is different for different elements depending on their position and orientation. Using the known mirror geometry, the shapes of the test pattern [Fig. 7(a)], and the position of the array with respect to the mirror, the distorted images of the array elements formed by the SPP mirror can be modeled and compared with the experiment [Fig. 7(d)]. These images show good agreement with each other. The SPP-formed images are rotated and stretched/compressed compared to the initial structure, but the shapes of the individual elements of the array can be clearly recognized. The additional broadening in the experimental image is related to the finite resolution of the microscope (the test pattern sizes of the order of 50 nm are comparable to the optical resolution of the appa-

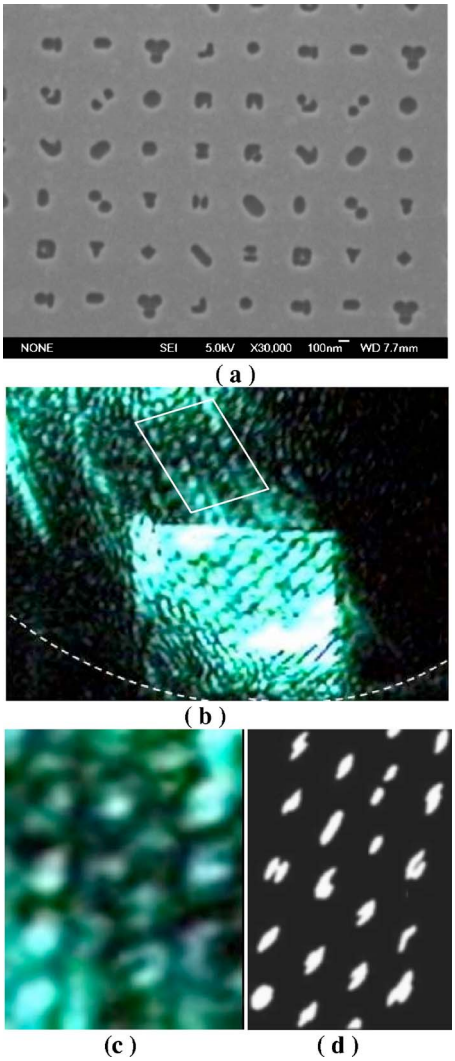


FIG. 7. (Color online) (a) SEM image of the aperiodic array in the metal film. (b) Large-scale image of the array obtained with SPP-assisted microscopy. Total size of the array is $20\times20$ $\mu$m$^2$. Droplet edge position is shown by the dashed line. Zoom of the marked area is shown at higher magnification in (c) together with the calculated image of the array using known position of the SPP mirror (d).

ratus), aberrations due to the imperfect mirror shape, and glycerin boundary quality.

A remarkable feature of the SPP-induced image in Fig. 7(b) is the apparent inverse character of magnification in this image. This behavior is clear from the comparison of Fig. 7(b) with Figs. 5(a) and 5(b), and also from Fig. 8 in which the magnification in this image is compared with a previously observed SPP-induced image of the triplet nanohole pattern. While in the SPP-induced image of the triplet array magnification grows with distance along the optical axis (which is consistent with a positive effective refractive index of the nanohole array), in the image of the aperiodic array magnification distribution is reversed. This behavior is consistent with negative sign of the effective refractive index of the nanohole array in Fig. 7(a). Thus, both signs of the refractive index may be realized in a magnifying SPP crystal mirror.

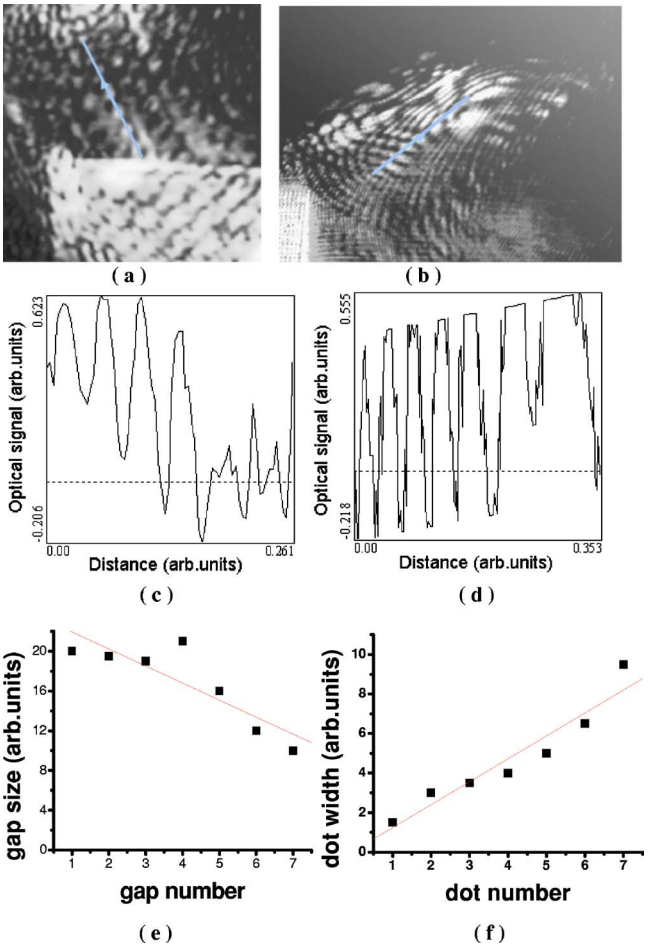


FIG. 8. (Color online) Comparison of magnification dependencies on the distance form the mirror edge in the SPP-induced image of the aperiodic array (a) and in the image of the triplet array (b). (c) and (d) show cross sections of the SPP-induced images. The cross-section directions are shown in (a) and (b), respectively. The corresponding plots of feature sizes in the images are shown in (e) and (f).

SPP-assisted microscope has the potential to become an invaluable tool in medical and biological imaging, where far-field optical imaging of individual viruses and DNA molecules may become a reality. Water droplets on a metal surface can be used as elements of 2D SPP optics in measurements where aqueous environment is essential for biological studies. The following experiments have been performed in order to illustrate these points. The SPP crystal mirror was used to image the T4 phage viruses[15] [Fig. 9(a)] and nanoscale polysterene spheres deposited onto the gold film patterned with a periodic array of doublet nanoholes.

Initial test experiments were performed with polystyrene spheres of various diameters in the nanometer-scale range. 200 nm diameter polystyrene spheres deposited on a metal surface were studied under the illumination with 502 nm light. The images taken in reflection [Fig. 9(b)] and transmission [Fig. 9(c)] shows that individual spheres, which have attached to the nanohole array surface as a result of the deposition process are clearly visible as standard luminous features. They appear to be bright in the transmission image

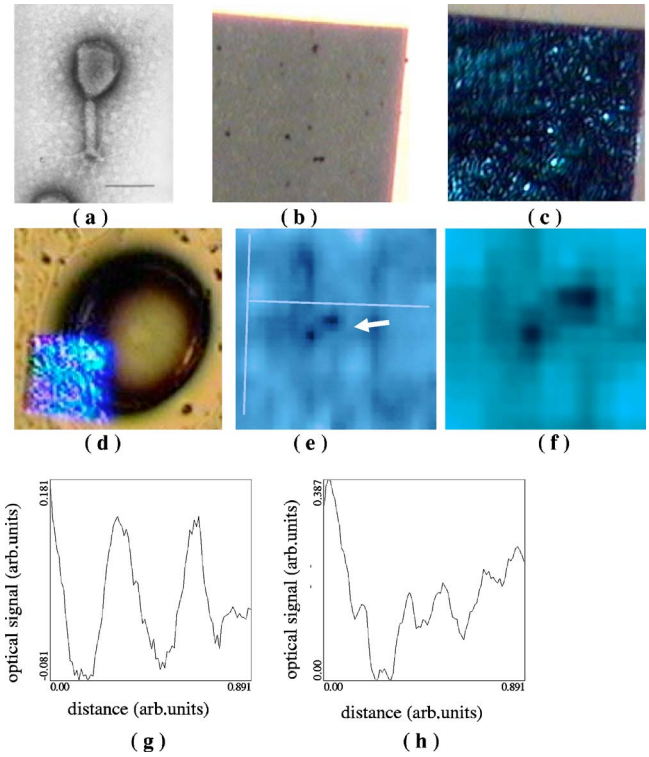


FIG. 9. (Color online) (a) Electron microscope image of the T4 phage. (b), (c) Optical images of the nanohole array with polystyrene spheres in reflection (b) and transmission (c) under illumination with 502 nm light. (d) The droplet used to form SPP mirror for imaging T4 phage. (e), (f) The images of T4 phage viruses visible as dark features (indicated by an arrow) in the SPP-induced image. Orthogonal cross sections (g) and (h) indicate resolving of the doublets in the SPP-induced image (e).

because they efficiently scatter SPP waves into photons. On the other hand, because they efficiently scatter SPPs in light, they must appear as dark features in the 2D SPP-induced images. Dark features of appropriate size indeed appeared in the SPP-formed images taken with the polysterene spheres (the same as T4 phage viruses). The size of the scatterers deposited onto a nanohole array can be estimated from the SPP-induced image via comparison with the periodicity of the nanohole array in the image. However, the quality of the SPP image of the nanoholes in the array appears to be somewhat worse in this case, compared to the images in Fig. 6 because of the increased scattering by the polystyrene spheres in glycerin.

Similar technique has been implemented in the experiments with the T4 phage viruses. Direct visualization of viruses by using far-field microscopy techniques would constitute an important development in biosensing. A typical T4 virus is around 200 nm long and 80–100 nm wide [Fig. 9(a) copied from Ref. 15]. In our experiments individual T4 viruses were deposited onto an array of doublet nanoholes (Fig. 6). After the glycerin droplet has been placed over the array [Fig. 9(d)] the SPP image demonstrates resolution of the individual 100 nm nanoholes separated by 40 nm gaps, as evidenced by the image cross sections [Figs. 9(g) and 9(h)] of the SPP image performed in the two orthogonal

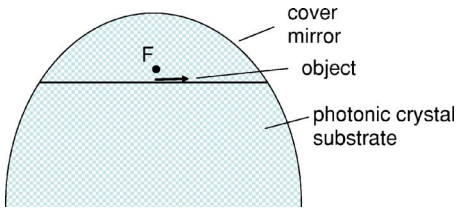


FIG. 10. (Color online) Schematic of a 3D magnifying photonic crystal mirror, which may be used in a 3D configuration of an immersion microscope based on photonic crystal materials.

directions, as shown in Fig. 9(e). In addition, the SPP-induced image contains dark features that are similar to the one shown in Figs. 9(e) and 9(f). While the surface density of these features was consistent with the T4 phage concentration in the deposited solution, the size of these features and their appearance was consistent with the way a T4 phage should look under a microscope with 50 nm resolution. Thus, the size, image sign (T4 phages appear as dark features), and image resolution in these experiments is consistent with the known geometry of the T4 phage viruses and the resolution of the SPP-assisted microscope.

## V. CONCLUSION

We have developed a theoretical model of the enhanced optical resolution of a far-field microscope based on optical elements made of 2D photonic and plasmon-polaritonic crystal materials, which uses propagating electromagnetic Bloch waves. The super-resolution is achieved due to coupling of evanescent components of the diffraction field generated by the object to the propagating Bloch modes of the photonic crystal space. The image magnification can be achieved by either using curved dielectric mirrors deposited onto the 2D photonic crystal, or by using the crystal boundary that is appropriately shaped to provide magnification for Bloch waves reflected from or refracted at the boundary. Both signs of the effective refractive index of a photonic crystal mirror have been observed in the experiments with SPP-assisted imaging. The technique was applied for imaging of various test patterns as well as viruses.

We should also point out that while 2D configuration of the SPP-assisted microscopy based on 2D photonic or SPP crystal mirrors offers some important advantages, such as relative ease of the structure fabrication, strong interaction between biological samples and SPP Bloch waves, etc., a 3D configuration of a microscope based on photonic crystal mirror is also possible. In this case, the evanescent components of the diffraction field generated by the object is coupled to the 3D photonic crystal Bloch modes but in contrast to the 2D case, the image is formed out of the surface plane. One of the potentially interesting configurations is shown in Fig. 10. In this configuration a photonic crystal mirror would consist of two parts, a substrate and a cover part, which would work together as a photonic crystal mirror. The plane separating these two parts should be close to the focal plane of the

mirror and filled with a very thin layer of index matching gel. If an object is positioned on the substrate and covered with the top mirror part, a magnified image of the object would be formed in free space, which may be viewed by a regular optical microscope. Operation of such microscope would be very similar to operation of a regular microscope. However, practical realization of this 3D microscope idea in the optical frequency range would require fabrication of high quality 3D photonic crystal materials.

## ACKNOWLEDGMENTS

This work has been supported in part by the NSF Grants Nos. ECS-0304046, CCF-0508213, and EPSRC (UK).

[1] J. B. Pendry, Phys. Rev. Lett. **85**, 3966 (2000).
[2] I. I. Smolyaninov, J. Elliott, A. V. Zayats, and C. C. Davis, Phys. Rev. Lett. **94**, 057401 (2005).
[3] V. Westphal and S. W. Hell, Phys. Rev. Lett. **94**, 143903 (2005).
[4] N. Fang, H. Lee, C. Sun, and X. Zhang, Science **308**, 534 (2005); D. O. S. Melville and R. J. Blaikie, Opt. Express **13**, 2127 (2005).
[5] S. A. Ramakrishna and J. B. Pendry, Phys. Rev. B **69**, 115115 (2004).
[6] I. I. Smolyaninov, C. C. Davis, J. Elliott, and A. V. Zayats, Opt. Lett. **30**, 382 (2005).
[7] A. V. Zayats, I. I. Smolyaninov, and A. Maradudin, Phys. Rep. **408**, 131 (2005).
[8] A. V. Zayats, J. Elliott, I. I. Smolyaninov, and C. C. Davis, Appl. Phys. Lett. **86**, 151114 (2005).
[9] H. Kosaka *et al.*, Appl. Phys. Lett. **74**, 1370 (1999); K. B. Chung and S. Hong, *ibid.* **81**, 1549 (2002).
[10] A. V. Zayats, I. I. Smolyaninov, W. Dickson, and C. C. Davis, Appl. Phys. Lett. **82**, 4438 (2003).
[11] M. Kretschmann and A. A. Maradudin, Phys. Rev. B **66**, 245408 (2002); M. Kretschmann, T. A. Leskova, and A. A. Maradudin, Opt. Commun. **215**, 205 (2003).
[12] S. A. Darmanyan and A. V. Zayats, Phys. Rev. B **67**, 035424 (2003).
[13] V. M. Agranovich, Y. R. Shen, R. H. Baughman, and A. A. Zakhidov, Phys. Rev. B **69**, 165112 (2004).
[14] I. I. Smolyaninov, J. Opt. A, Pure Appl. Opt. **7**, S165 (2005).
[15] The Universal Virus Database of the International Committee on Taxonomy of Viruses.